Properties and Thermal Degradation Kinetics of Polystyrene/Organoclay Nanocomposites Synthesized by Solvent Blending Method: Effect of Processing Conditions and Organoclay Loading

S. V. Krishna, G. Pugazhenthi

Department of Chemical Engineering, Indian Institute of Technology Guwahati, Guwahati 781039, Assam, India

Received 28 May 2010; accepted 10 August 2010
DOI 10.1002/app.33179
Published online 23 November 2010 in Wiley Online Library (wileyonlinelibrary.com).

ABSTRACT: In this study, intercalated/exfoliated polystyrene (PS)/organoclay nanocomposites containing different concentration of organoclay have been prepared via solvent blending method, using xylene as a solvent. Some resulting intercalated nanocomposites are transformed to exfoliated nanocomposites by increasing the refluxing temperature or refluxing time for a constant organoclay loading. The X-ray diffraction results reveal the formation of intercalation/exfoliation of organoclay in the PS matrix. The Fourier transform infrared spectroscopy and transmission electron microscopy results confirm the presence of nanomaterial in PS/organoclay nanocomposites. Completely exfoliated nanocomposites are achieved by decreasing the content of organoclay and elongating the refluxing temperature or refluxing time. Thermogravimetric analysis data show that the PS/organoclay nanocomposites have significant enhanced thermal stability. When 50% weight loss is selected as a point of comparison, the thermal decomposition temperature (T_d) of the exfoliated PS/organoclay nanocomposites with 7 wt % of organoclay is 17°C higher than that of pure PS. Thermal decomposition temperature of exfoliated PS/organoclay nanocomposites is better than that of intercalated nanocomposites for a constant organoclay loading. The glass transition temperature (T_g) of PS/organoclay nanocomposites is ~ 7.1–8.6°C higher than that of pure PS. The thermal degradation activation energy of the nanocomposites is determined via Coats-Redfern method. The improvement of thermal stability of nanocomposites is also confirmed by increasing the activation energies (E_a) and the integral procedural decomposition temperature. Criado method is finally used to determine the degradation reaction mechanism of various samples. The water uptake capacity of PS/organoclay nanocomposites is negligible when compared with pure PS. © 2010 Wiley Periodicals, Inc. J Appl Polym Sci 120: 1322–1336, 2011

Key words: polystyrene; organoclay; nanocomposites; solvent blending; thermal stability

INTRODUCTION

Polymer/clay nanocomposites are now an active area of research because of its enhanced physical, mechanical, and chemical properties when compared with those of pure polymer.[1,2] Polymer/clay nanocomposites comprise dispersions of nanoclay platelets throughout a polymer matrix. Clay minerals, especially montmorillonite (MMT), are the most widely chosen nanofiller for the preparation of polymer/clay nanocomposites due to some advantages. MMT clay has a special layer structure in which the thickness of the clay platelet is <1 nm and the length of the surface is in the order of 300 nm; the clay platelets are stacked together to form the tactoids.[3] Moreover, clays have negative charges in the surface that are compensated by the naturally occurring cations like Na^+, K^+, and Ca^{2+} situated in the interlayer position. These cations can be exchanged by other cations under suitable condition. Generally, clays do not mix with the polymer because clays are hydrophilic inorganic compound whereas polymer contains hydrophobic group. Therefore, clays are to be modified by organic modifier containing both hydrophilic and long-chain hydrophobic group, mostly by ammonium ions having long alkyl chains, to increase not only the interlayer spacing but also the compatibility with the polymer matrices. Besides this, clay is naturally occurring, environment friendly, cheap, and readily available in large quantities. Polymer/clay nanocomposites have a weight advantage over conventional microcomposites as they require only 0.5–7% by weight of clay loading to achieve substantial improvement in thermal and mechanical properties, compared with conventional composites with 10–50% by weight of filler loading.[4,5] Besides nanoclay, carbon nanotubes have also shown a high potential to improve the mechanical and electrical properties of the polymer.[6] But carbon nanotube has not been widely used to improve the mechanical properties because of its high material cost.

Two main types of polymer/clay nanocomposites are obtained when the nanoclays are dispersed in a polymer matrix, which include intercalated and

Correspondence to: G. Pugazhenthi (pugal@iitg.ernet.in).

exfoliated. Intercalation results from the penetration of polymer chains into the interlayer region and interlayer expansion. The ordered structure layer is preserved and can be detected by X-ray diffraction (XRD). In contrast, exfoliation involves extensive polymer penetration and silicate platelets delamination. In this case, the ordered structure layer is not preserved, i.e., the individual platelets are randomly dispersed in the polymer matrix and cannot be detected by XRD. From the structural point of view, exfoliated nanocomposites are expected to have better properties than intercalated ones.[7] Various techniques involved for dispersing clay at a nanoscopic scale include melt compounding, *in situ* polymerization, emulsion/suspension polymerization, and solvent blending. Among these methods, solvent blending has been a widely used technique, and it is one of the approaches that consistently give exfoliated materials, provided the clay organic treatment, solvent, and blending conditions are considered.[8,9]

Polystyrene (PS) is an important engineering thermoplastic. It is a strong plastic, which can be easily injected, extruded, or blow molded thus making it a very useful and versatile manufacturing material. A series of nanocomposites consisting of PS polymer and clays have been appeared in the literatures, which have been prepared via different techniques. Recently, Qu et al.[10] developed exfoliated PS/layered double hydroxide (LDH) nanocomposites via emulsion polymerization. They reported that the decomposition temperature of exfoliated PS/LDH sample with 5 wt % LDH loading was 19°C higher than that of pure PS when 50% weight loss was selected as a point of comparison. Ding et al.[11] prepared PS/MMT nanocomposites by free radical polymerization method. The thermal decomposition temperature and glass transition temperature of the nanocomposite were 9 and 3°C, respectively, higher than that of pure PS. Qiu et al.[12] developed the exfoliated PS/ZnAl LDH nanocomposites by solution intercalation method. The exfoliation of LDH into the PS matrix was confirmed by XRD and transmission electron microscopy (TEM) analysis. The thermal decomposition temperature of the nanocomposites was 16°C higher relative to pure PS. In the work of Wang et al.,[13] they showed that the thermal stability of the PS/organophilic MMT (OMMT) nanocomposites prepared by free radical polymerization increased with OMMT loading and was 10–50°C higher than that of pure PS. They have also prepared the polymer-clay nanocomposite of styrene and methyl methacrylate by bulk, solution, suspension, and emulsion polymerization.[14] The obtained exfoliated PS-clay nanocomposites exhibited superior mechanical properties than that of the pure PS. Yeh et al.[15] also reported the series of PS/MMT nanocomposites synthesized by *in situ* thermal polymerization method, and they showed enhanced thermal stability and anticorrosive properties over neat polymer.

Tseng et al.[16] prepared PS-clay nanocomposites by free radical polymerization of the styrene containing intercalated OMMT. The exfoliated nanocomposites have higher thermal stability and better mechanical properties than the pure PS. Doh and Cho[17] reported on the synthesis of intercalated PS containing dispersed OMMT that exhibited higher thermal stability relative to the pure PS or the PS/pristine MMT composite. Liu et al.[18] demonstrated that the thermal decomposition temperature of PS/OMMT nanocomposite samples containing 5% OMMT was 25°C higher than that of pure PS. Kim et al.[19] developed intercalated syndiotactic PS/organophilic clay nanocomposites by direct-melt intercalation method using thermally stable alkyl phosphonium modified clay. The crystallization rate of the nanocomposites does not increase despite the presence of clay, which may be because of the physical hindrance of organic modifiers in the clay dispersion. However, the nanocomposites exhibited enhanced mechanical and thermal properties relative to the virgin polymer. Qi et al.[20] also reported that the PS/OMMT nanocomposites prepared by *in situ* polymerization has higher weight-average molecular weights, lower glass-transition temperatures, and better thermal stability (the decomposition temperature was improved by ~ 70°C) than the virgin PS.

Many researchers have investigated the thermal degradation kinetics of the nanocomposite material.[21–25] Lesnikovich et al. examined the kinetics of oxidative degradation of flame-retardant polyesters [poly(ethylene terephthalate)][21] and also the effect of hexabromocyclododecane as a fire-retardant additive on polypropylene (PP) thermal degradation.[22] Wang and coworkers[23–25] systematically investigated the thermal oxidative degradation behavior of poly(ethylene terephthalate) and its blend with MMT nanocomposite. Very few studies on the thermal or thermo-oxidative degradation kinetics of the flame-retarded PP with intumescent flame-retardants (IFRs), e.g., Neininger et al.[26] used a mathematical model, i.e., simplified kinetic scheme, to predict the global kinetics of the thermal degradation of IFRs added in textile-reinforced composite. They investigated the influence of the increased heating rates on the char yield and also the relationship between the Arrhenius parameters of volatile-forming reaction and those of char-forming reaction.

The above extensive literature review clearly indicates that there are many factors such as processing conditions and synthetic method that influence the nanostructure of polymer/clay nanocomposites. In solvent blending method, the processing conditions predominantly play a major role on the properties of

the polymer/clay nanocomposites. Therefore, in this article, we address the effect of synthesizing conditions such as refluxing temperature and duration on the structural and thermal properties of the PS/organoclay nanocomposites derived via solvent blending method. In addition, the effect of organoclay loading on the properties of the PS nanocomposite is also investigated. Based on the thermogravimetric (TG) analysis (TGA) data, the kinetic parameters of thermal decomposition of PS nanocomposites such as apparent activation energy (E_a), pre-exponential factor (A), and apparent reaction order (n) are calculated using Coats-Redfern method. Thermal decomposition reaction mechanism of the PS nanocomposites is also examined using Criado method. In addition, an investigation for the nanocomposites is carried out by evaluating the integral procedural decomposition temperature (IPDT), a thermal stability factor of the nanocomposites.

KINETICS OF THERMAL DEGRADATION

The overall rate of polymer degradation is commonly described by the Eq. (1).[27]

$$\frac{d\alpha}{dt} = A\exp\left(-\frac{E_a}{RT}\right)f(\alpha) \tag{1}$$

where α is the conversion degree or fractional weight loss, t is the reaction time, T is the temperature, R is the gas constant, A is the pre-exponential factor, E_a is the apparent activation energy, and $f(\alpha)$ is the reaction model.

If the constant heating rate of TGA process is set as $\beta = dT/dt$, the conversion degree α can be expressed as the function of the temperature. However, the temperature is dependent on the heating time. Therefore,

$$\frac{d\alpha}{dt} = \frac{d\alpha}{dT}\frac{dT}{dt} = \beta\frac{d\alpha}{dT} \tag{2}$$

β is the heating rate in TGA. The combination of eq. (1) with (2) gives the following relationship

$$\frac{d\alpha}{dT} = \frac{A}{\beta}\exp\left(-\frac{E_a}{RT}\right)f(\alpha) \tag{3}$$

Integration of the both sides of above equation and rearrangement gives

$$g(\alpha) = \int_0^\alpha \frac{d\alpha}{f(\alpha)} = \frac{A}{\beta}\int_0^T \exp\left(-\frac{E_a}{RT}\right)dT \tag{4}$$

where, $g(\alpha)$ is the integral function of conversion degree α. As far as the polymer is concerned, its degradation process, generally, obeys the sigmoidal or deceleration functions. For different solid reaction mechanism, $g(\alpha)$ has different expressions (Table I).[27] These expressions can be used to predict the solid reaction mechanism reflected by the dynamic TG curves.

Coats-Redfern method

Coats-Redfern method uses the following relations in [eq. (4)]:

$$g(\alpha) = \int_0^\alpha \frac{d\alpha}{f(\alpha)} = \frac{A}{\beta}\int_0^T \exp\left(-\frac{E_a}{RT}\right)dT = \int_0^\alpha \frac{d\alpha}{(1-\alpha)^n} \tag{5}$$

where, $f(\alpha) = (1-\alpha)^n$

Let $x = E_a/RT$, and after rearranging, eq. (5) becomes

$$g(\alpha) = \frac{ART^2}{\beta E_a}\left(1-\frac{2RT}{E_a}\right)\exp(-\frac{E_a}{RT}) \tag{6}$$

According to eq. (5), $g(\alpha)$ can be written as different expressions at different n values.

When $n = 1$,

$$g(\alpha) = -\ln(1-\alpha) \tag{7a}$$

when $n \neq 1$,

$$g(\alpha) = \frac{1}{n-1}\left[(1-\alpha)^{1-n} - 1\right] \tag{7b}$$

The combination of eq. (6) with eq. (7) followed by the rearrangement obtains,

$$\mathrm{n} = 1\ln\left(-\frac{\ln(1-\alpha)}{T^2}\right) = \ln\left[\frac{AR}{\beta E_a}\left(1-\frac{2RT}{E_a}\right)\right] - \frac{E_a}{RT} \tag{8a}$$

$n \neq 1$

$$\ln\left(\frac{1-(1-\alpha)^{1-n}}{T^2(1-n)}\right) = \ln\left[\frac{AR}{\beta E_a}\left(1-\frac{2RT}{E_a}\right)\right] - \frac{E_a}{RT} \tag{8b}$$

where n is reaction order. Generally, the logarithmic term on the right part of the above equations is regarded as constant. Then, the determination of the reaction order, n can be done by linear fitting of the left part of above equations dependence of $-1/T$. The n value at the best correlation coefficient (R) obtained is the real reaction order, and the apparent activation energy E_a and pre-exponential factor A can be hereby calculated.

Criado method

Criado et al. proposed a method that can accurately determine the reaction mechanism in the solid reaction process using the activation energy value.

TABLE I
The Expressions of $g(\alpha)$ for the Most Frequently Used Reaction Mechanism of Solid State Processes[28]

Mechanism	$g(\alpha)$	Solid state process
Sigmoidal function		
A_2	$[-\ln(1-\alpha)]^{1/2}$	Nucleation and growth: Avrami eq. (1)
A_3	$[-\ln(1-\alpha)]^{1/3}$	Nucleation and growth: Avrami eq. (2)
A_4	$[-\ln(1-\alpha)]^{1/4}$	Nucleation and growth: Avrami eq. (3)
Deceleration function		
R_2	$[1-(1-\alpha)^{1/2}]$	Phase boundary controlled reaction: contraction area
R_3	$[1-(1-\alpha)^{1/3}]$	Phase boundary controlled reaction: contraction volume
D_1	α^2	One-D diffusion
D_2	$(1-\alpha)\ln(1-\alpha)+\alpha$	Two-D diffusion
D_3	$[1-(1-\alpha)^{1/3}]^2$	Three-D diffusion: Jander equation
D_4	$(1-(2/3)\alpha)-(1-\alpha)^{2/3}$	Three-D diffusion: Ginstlinge–Brounshtein equation
F_1	$-\ln(1-\alpha)$	Random nucleation having one nucleus on individual particle
F_2	$1/(1-\alpha)$	Random nucleation having two nucleus on individual particle
F_3	$1/(1-\alpha)^2$	Random nucleation having two nucleus on individual particle

$$Z(\alpha)=\frac{\frac{d\alpha}{dt}}{\beta}\pi(x)T \tag{9}$$

where, $x = E_a/RT$ and $\pi(x)$ is an approximate expression obtained by integration against temperature, which cannot be expressed by simple analysis formulas. The reasonable relationship between $\pi(x)$ and $P(x)$ is reported elsewhere[27]:

$$\pi(x)=xe^xP(x) \tag{10}$$

where $P(x)$ is expressed as:

$$P(x)=\frac{\exp(-x)}{x}\frac{x^3+18x^2+86x+96}{x^4+20x^3+120x^2+240x+120} \tag{11}$$

When $x > 20$, eq. (11) can give error $<10^{-5}\%$, which is the basis for analyzing the TG data. Combining eqs. (2), (9), and (10), the following relationship is obtained:

$$Z(\alpha)=f(\alpha)g(\alpha) \tag{12}$$

The combination of eq. (3) with (12) results in the following equation:

$$Z(\alpha)=\frac{\beta}{A}g(\alpha)\frac{d\alpha}{dT}\exp\left(\frac{E_a}{RT}\right) \tag{13}$$

From eqs. (2), (9), and (10), the following relationship can also be obtained:

$$Z(\alpha)=\frac{d\alpha}{dT}\frac{E_a}{R}\exp\left(\frac{E_a}{RT}\right)P(x) \tag{14}$$

Equation (13) is used to plot the master $Z(\alpha)$-α curve of the different reaction mechanisms shown in Table I, and eq. (14) is used to plot the experimental $Z(\alpha)$-α curve according to the TG data. The comparison of the master $Z(\alpha)$-α curve with the experimental $Z(\alpha)$-α curve can easily and accurately predict the reaction mechanism of the thermal degradation reaction.

Integral procedure decomposition temperature

IPDT is a thermal stability factor of the nanocomposites, which is correlated to the volatile parts of the polymeric materials.[28] IPDT is determined on the basis of the overall shape of the TGA curve. Therefore it can estimate the overall inherent thermal stability for the decomposition proceeded in a single or several consecutive steps. A schematic diagram of a typical TGA thermogram revealing the areas of A_1, A_2, and A_3 is shown in Figure 1 for the determination of IPDT. The value of IPDT is calculated as follows:

$$\mathrm{IPDT}=[(A_1+A_2)^3/A_1(A_1+A_2+A_3)^2](T_f-T_i)+T_i \tag{15}$$

where, T_i and T_f are the beginning of test temperature and the end of test temperature of the TGA measurement, respectively.

EXPERIMENTAL

Materials

PS supplied by National Chemicals, Vadodara, India, and organically modified clay, CRYSNANO-1060 supplied by Crystal Nanoclay Private Limited (Pune, Merck, Mumbai) India, were used throughout this work. Xylene procured from Merck, India, was used as received without further purification.

Preparation of PS/clay nanocomposites

PS/organoclay nanocomposites were prepared via solvent blending method in which xylene was used as a solvent. Both the PS and organoclay were dried

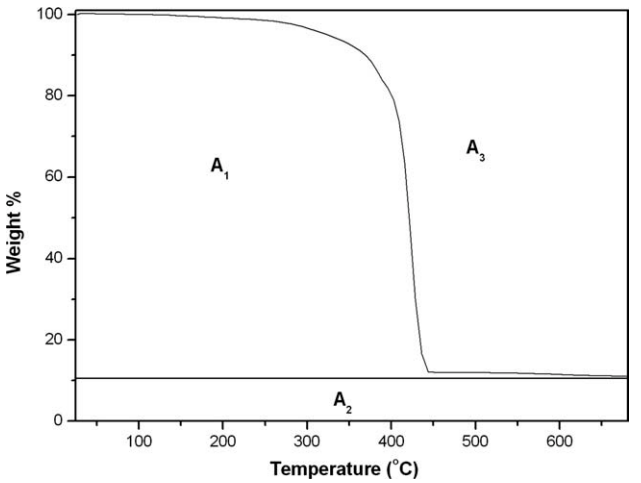

Figure 1 Schematic diagram of Doyle's method for determining IPDT.

in a vacuum oven at 80°C to remove moisture. A given amount of organoclay was dispersed in 50 mL of xylene with continuous stirring for 24 h at desired temperature. After that, estimated quantity of PS was added into the above organoclay solution and refluxed for desirable time at the same temperature. Then the resulting PS/organoclay solution was spread over a glass plate and left for 24 h in ambient temperature yielding a viscous gel layer. Finally, the film was heated in an oven for 6 h at 100°C to remove the remaining solvent to obtain PS/organoclay nanocomposites. The pure PS film was also prepared by an identical procedure in the absence of organoclay. The prepared nanocomposite films were characterized for structural and thermal properties. To study the effect of nanomaterial loading, various PS/organoclay nanocomposites were prepared with 3, 5, 7, and 20 wt % of organoclay at constant temperature (25°C) and refluxing time (12 h). The weight percentage of organoclay in the nanocomposites was represented by polymer; for example, PSNC (3, 25, 12) indicates PS/organoclay nanocomposite prepared using 3 wt % organoclay at 25 °C with refluxing duration of 12 h. Similarly, the effect of refluxing time and temperature on the properties of nanocomposites were studied for a constant nanomaterial loading of 5 and 7 wt %, respectively. The conditions and composition used to prepare PS/organoclay nanocomposites were presented in Table II.

Characterization

XRD profile of organoclay and PS/organoclay nanocomposite samples was recorded under air at room temperature using AXS D8 ADVANCE Fully Automatic Powder X-Ray Diffractometer (Bruker) equipped with a Cu-Kα radiation (λ = 0.15418 nm) and Ni filter. The patterns were acquired for 2θ range of 2° to 50° with a scan speed of 0.05° s^{-1}. The transmission electron microscopy image was obtained on a JEOL JEM-2100 transmission electron microanalyzer with an accelerating voltage of 200 kV. To confirm the presence of organoclay in PS/organoclay nanocomposites, the nanocomposite samples were analyzed using Perkin–Elmer Fourier transform infrared spectroscope (FTIR). The TGA for thermal stability was performed under nitrogen atmosphere on a TGA/SDTA851e/LF/1100 model (Mettler Toledo, Greifensee, Switzerland) instrument using a heating rate of 10°C/min from 25 to 700°C. A Mettler Toledo-1 series differential scanning calorimetry (DSC) was used to examine the glass transition temperature of the PS/organoclay nanocomposites. Samples were heated from 40 to 150°C at a rate of 5°C/min under nitrogen atmosphere.

The water uptake test was considered as a standard method to evaluate the water resistance of the nanocomposite films using gravimetric method. Water uptake of the nanocomposite films were determined by measuring the change in the weight before and after the hydration. Five samples of each nanocomposite films (having dimensions of 3 × 3 cm) were dried at 100°C for 4 h to bring each sample to an identical starting state. The nanocomposite samples were then weighed to note the dry weight. Finally, the dried samples were soaked in water for 48 h. Then they were taken out, wiped with tissue paper, and weighed immediately. The water uptake of the nanocomposite films were calculated by using the eq. (16).

$$\text{Water uptake}(\text{wt}\%) = \frac{W_w - W_d}{W_d} \times 100 \qquad (16)$$

where, W_w and W_d are the weights of wet and dry nanocomposite films, respectively.

RESULTS AND DISCUSSION

XRD analysis

The XRD is an effective tool to characterize the types of the layered structure, i.e., intercalated and/or exfoliated polymer/organoclay nanocomposites, because the peak changes with the gallery height of the organoclay. The d_{001} spacing was calculated from peak positions using Bragg's law: $n\lambda = 2d \sin\theta$, where λ is the X-ray wave length (1.5418 Å). For organoclay and PS/organoclay nanocomposites, the diffraction peaks in 2θ = 2–50° were recorded. In the case of intercalated nanocomposites, a XRD peak is seen at larger *d*-spacing than in the pristine clay, whereas in case of exfoliated structure, no peak is seen. Figure 2 depicts the XRD patterns of pure PS,

TABLE II
Preparation Condition and Composition of PS/Organoclay Nanocomposites

Name of sample	Organoclay content (wt %)	PS content (wt %)	Temperature (°C°C)	Refluxing time (h)
PSNC (3, 25, 12)	3	97	25	12
PSNC (5, 25, 12)	5	95	25	12
PSNC (7, 25, 12)	7	93	25	12
PSNC (20, 25, 12)	20	80	25	12
PSNC (5, 25, 6)	5	95	25	6
PSNC (7, 110, 12)	7	93	110	12

Values within parenthesis in sample column represents loading (wt %), refluxing temperature (°C), and refluxing time (h), respectively.

organoclay, and PS/organoclay nanocomposites prepared with various organoclay loading. It is observed that the pure organoclay shows a peak (d_{001}) at $\sim 2.5°$, corresponding to a basal spacing of 3.53 nm. The basal spacing of organoclay in the PS nanocomposites increases to >3.60 nm from 3.53 nm of the original clay layers with decreasing content of organoclay to 20 wt % from 100 wt % because of the intercalation of PS molecule into the clay layers. In case of intercalated nanocomposite, a single extended polymer chain can penetrate between the silicate layers, a well-ordered multilayer morphology results with alternating polymeric and inorganic layers. The diffraction peak becomes weaker with further decreasing the clay content to 7 wt %. When the clay loading is <5 wt %, no diffraction peak is observed, as shown in Figure 2. These data illustrate that the equilibrium between exfoliation and intercalation structures in the PS/organoclay nanocomposites can be driven toward to exfoliation by decreasing the content of organoclay. Qiu et al.[12] have also obtained completely exfoliated PS/ZnAl-LDH nanocomposites by decreasing the LDH content to <5 wt %. Wang et al.[13] achieved the exfoliated structure of PS/MMT nanocomposites (prepared by free radical polymerization) with 1 and 2 wt % MMT loading, whereas intercalated structure obtained with MMT content >3 wt %. In the work reported by Yeh et al.,[15] PS/MMT nanocomposites prepared by *in situ* polymerization formed exfoliated structure with 1 wt % MMT loading and higher nanomaterial loading (5 and 10 wt %) yielded intercalated structure.

The XRD patterns of the pure PS, organoclay, and PS/organoclay nanocomposites prepared using different refluxing time are shown in Figure 3. It can be seen that the basal spacing of d_{001} peak of the clay layers in the PS nanocomposite increases to 3.84 nm from 3.53 nm of the original clay layers, after refluxing for 6 h at 25°C with 5 wt % of organoclay loading. This means that clay layers in the nanocomposite are intercalated. However, the diffraction peak (001) disappears when the refluxing time increases to 12 h for a constant nanomaterial loading and temperature. It means that the clay layers in the nanocomposites are completely exfoliated. This implies that the basal spacing of the nanomaterial in the nanocomposite increases with the refluxing time. Similar trend was also observed by Qiu et al.[12] for the PS/ZnAl-LDH nanocomposites.

Figure 4 illustrates the XRD patterns of pure PS, organoclay, and PS/organoclay nanocomposites

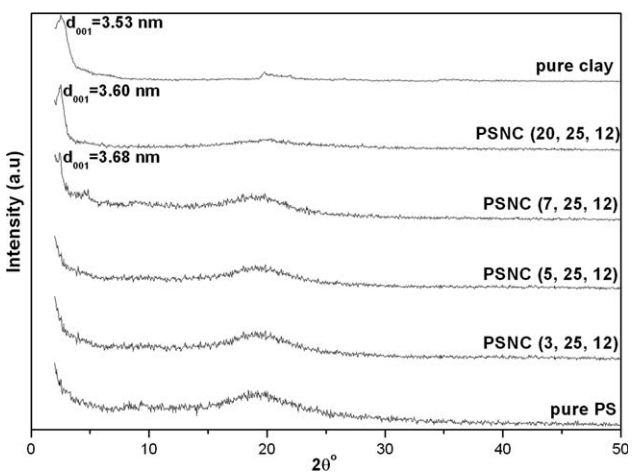

Figure 2 Effect of organoclay loading on the structure of PS/organoclay nanocomposites characterized by XRD.

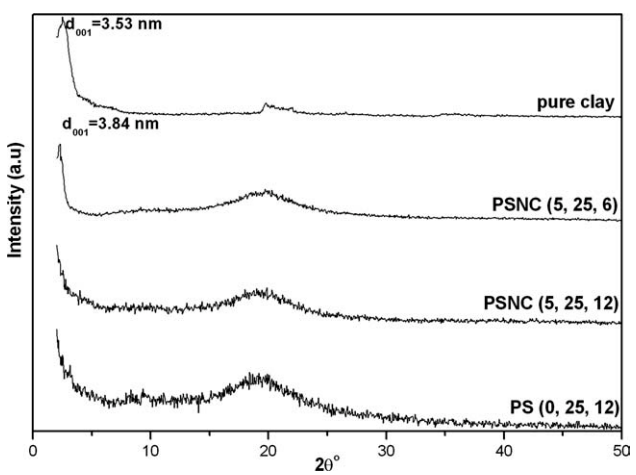

Figure 3 Effect of refluxing time on the structure of PS/organoclay nanocomposites characterized by XRD.

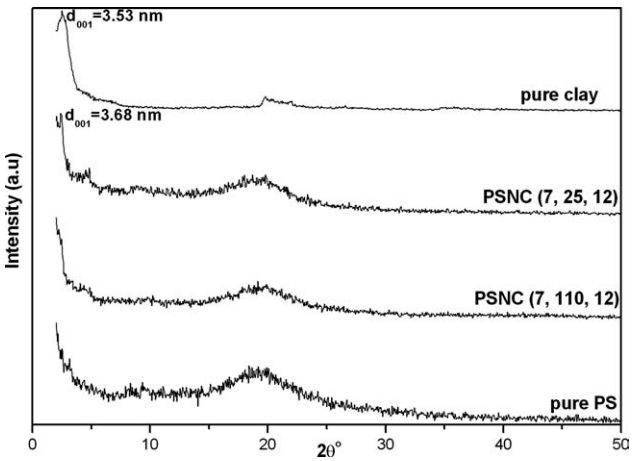

Figure 4 Effect of refluxing temperature on the structure of PS/organoclay nanocomposites characterized by XRD.

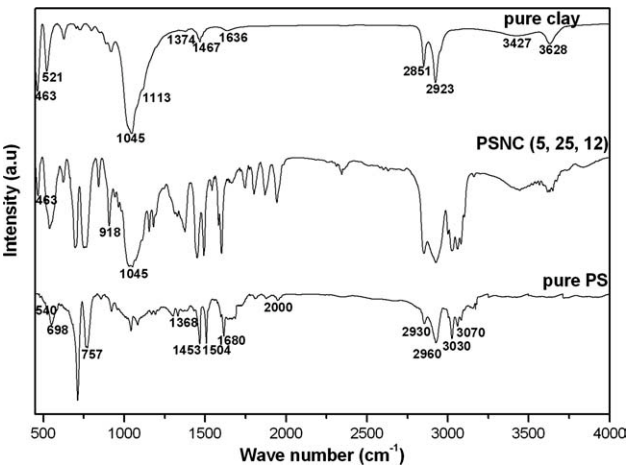

Figure 5 FTIR spectrum of pure organoclay, pure PS and PS/organoclay nanocomposite.

prepared at different refluxing temperatures. It can be seen that the basal spacing of d_{001} peak of the clay layers in the nanocomposites increases to 3.68 nm from 3.53 nm of the original clay layers, after refluxing for 12 h at 25°C with 7 wt % of nanomaterial. This means that clay layers in the nanocomposite have been intercalated. When the refluxing temperature increased to 110°C, the diffraction peak completely disappears for a constant refluxing time and nanomaterial loading. This implies that refluxing at high temperature can form an exfoliated PS/organoclay nanocomposite because the silicate layers are completely dispersed in a continuous polymer matrix. The main reason for the development of PS/organoclay nanocomposites structure from intercalated to exfoliated is that more and more clay layers broke into small fragments as refluxing temperature increased and thus form an exfoliated structure of nanocomposites. Table III presents the complete XRD results of PS/organoclay nanocomposites.

FTIR analysis

FTIR spectrum of pure organoclay, pure PS, and PS/organoclay nanocomposite is shown in Figure 5. Table IV illustrates the infrared band assignments of pure organoclay and pure PS.[13] The FTIR spectrum of the PS/organoclay nanocomposite shown in Figure 5 clearly exhibits the characteristic absorptions attributable to both the polymeric organic and inorganic groups. This indicates that the clay layers are dispersed into the PS matrix to form the PS/organoclay nanocomposite. Compared with pure PS, the PS/organoclay nanocomposite shows some new peaks in the region of 1045, 918, and 463 cm^{-1} correspond to Si—O stretching vibration, Al—O stretching, and Mg—O bending vibrations of organoclay, respectively. These peaks indicate the existence of organoclay in PS/organoclay nanocomposite. Similar types of results are also obtained for all other PS/organoclay nanocomposites (Fig. 6) prepared using various organoclay loading. It is evidenced from Figure 6 that as the loading of clay increases, the intensities of the clay bands (1045, 918, and 463 cm^{-1}) become stronger in the FTIR spectrum of the PS/organoclay nanocomposites.

TABLE III
XRD Results of Pure Organoclay and PS/Organoclay Nanocomposites

Name of sample	2θ°	d_{001} (nm)	Structure
Pure 1060	2.5	3.53	----
PSNC (3, 25, 12)	Disappear	----	Exfoliated
PSNC (5, 25, 12)	Disappear	----	Exfoliated
PSNC (7, 25, 12)	2.4	3.68	Intercalated
PSNC (20, 25, 12)	2.45	3.60	Intercalated
PSNC (5, 25, 6)	2.4	3.84	Intercalated
PSNC (7, 110, 12)	Disappear	----	Exfoliated

Transmission electron microscopy

The morphological structure of the nanocomposite is further studied by the TEM analysis. Figure 7(a) shows the TEM image of exfoliated PS/organoclay nanocomposite prepared with 7 wt % of nanomaterial loading at 110°C. In case of exfoliated PS/organoclay nanocomposite, it can be seen that the clay layers [dark part in Fig. 7(a)] are homogeneously dispersed with face-face orientations in the PS matrix (bright part). The photograph shows the lamellar structure of organoclay exfoliated by the PS macromolecular chain; the lines of the layers are shown using arrow marks. The XRD data shown in Figure 4 also confirm that the clay layers in the PS nanocomposite sample are completely exfoliated as mentioned above. Therefore, it is reasonable to describe this sample as exfoliated. TEM image [Fig. 7(b)] of the PS/organoclay nanocomposite (7, 25, 12)

TABLE IV
FTIR Band Assignments of Pure Organoclay and Pure PS

Source	Frequency (cm^{-1})	Assignment
Pure organo clay	521 and 463	Al-—O stretching and Mg—-O bending vibrations
	1113 and 1045	Si—-O out of plane and in-plane vibrations
	1374	Symmetric CH_2 wagging and some C—-C stretching
	1636	Bending vibrational mode of hydrated water molecules and weakly bonded water molecules
	2923, 2851, and 1467	CH_2 asymmetric stretching, symmetric stretching, and in-plane scissoring vibrations
	3628 and 3427	Two types of O—-H groups: isolated OH groups and those involved in hydrogen bonding
Pure PS	3070 and 3030	Aromatic C—-H stretching vibration
	2960 and 2930	Aliphatic C—-H stretching vibration
	2000 and 1680	Weak aromatic overtone and combination band
	1504 and 1496	C=C stretching vibration
	1453 and 1368	CH_2 bending vibrations
	757 and 698	CH out-of-plane bending of the phenyl ring or mono substituted benzene
	540	Out-of-plane deformation of the phenyl ring

synthesized with 7 wt % of nanomaterial loading at 25°C reveals the formation of intercalated structure of the nanocomposite.

Thermal properties

Thermogravimetric analysis

The TGA provides important proofs in determining the thermal stability of the nanocomposites. Figure 8 illustrates the TGA curves for pure organoclay, pure PS, and PS/organoclay nanocomposites with various amounts of clay content. The thermal decomposition of pure PS sample occurs in the range of 350–450°C. Generally, the PS/organoclay samples exhibit two different types of weight losses. The first step of weight loss at ~ 150–350°C is because of the evaporation of physically absorbed water and thermal decomposition of the alkyl chains of surfactant molecules present between the interlayer of organoclay.

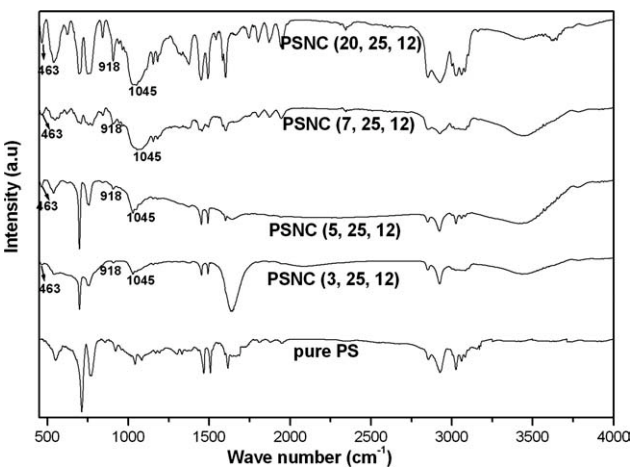

Figure 6 FTIR spectrum of the PS nanocomposites with various amount of clay loading.

The second step of weight loss appears at the temperature range of 350–480°C because of thermal degradation of PS chains and the formation of black charred residues. The degradation rate in this step is much slower compared with pure PS. This beneficial effect can be due to the hindered effect of clay layers for the diffusion of volatile products throughout the composite material. After 500°C, all the curves become flat and the inorganic residue mainly remained. When 15% weight loss is selected as a point of comparison, the thermal decomposition temperature for pure PS, PS/organoclay nanocomposites samples containing 3, 5, 7, and 20 wt % of clay is determined as 393, 373, 382, 384, and 386°C, respectively. It clearly demonstrates that the thermal decomposition temperature of nanocomposites is relatively lower than that of pure PS. The surfactant used for modification of clay is likely responsible for the initial destabilization of the nanocomposites. However, PS/organoclay nanocomposites show better thermal stability at high temperatures (>400°C), which is confirmed by shifting of the TGA curve of PS/organoclay nanocomposites toward right of the TGA curve for pure PS (Fig. 8). When 50% weight loss is selected as a point of comparison, the thermal decomposition temperature for pure PS, PS/organoclay nanocomposites samples containing 3, 5, 7, and 20 wt % of clay is found to be 410, 423, 426, 425, and 421°C, respectively. It can be seen that the thermal decomposition temperature of PS/organoclay nanocomposites is 11–16°C higher than that of pure PS, in which the PS/organoclay nanocomposite with 5 wt % has the best thermal stability. The excess loading of clay (e.g., 7 and 20 wt %), can make the nanocomposites to decrease the thermal stability. The most probable reason is that the relatively large organic surfactant content of the composites produced less stable charred layers during the

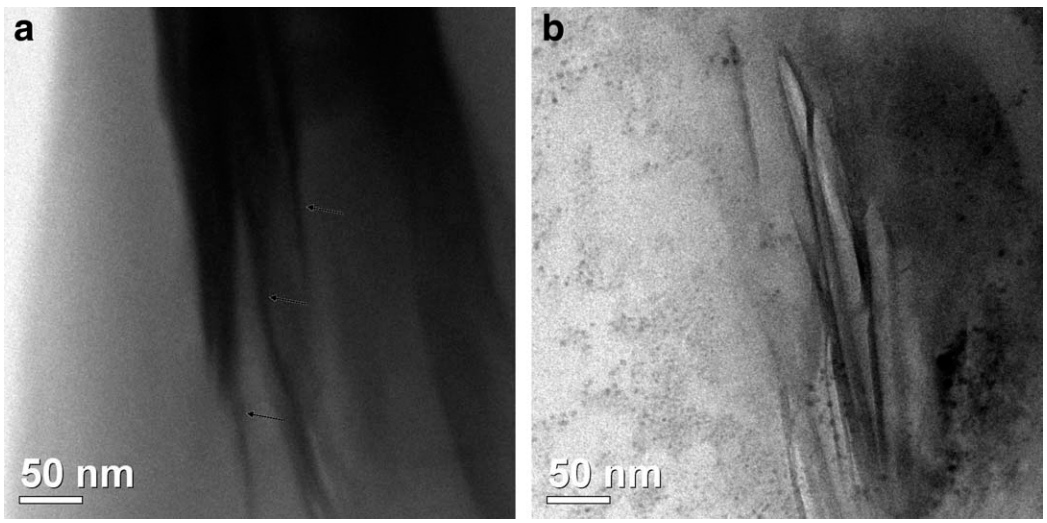

Figure 7 TEM images of PS/organoclay nanocomposite prepared at 110°C with 7 wt % of organoclay loading (a) and prepared at 25°C with 7 wt % of organoclay loading (b).

decomposition.[29] Very similar behavior has already been observed in some polymer/silicates[30,31] and polymer/LDH[12] nanocomposites. The enhanced thermal stability of PS nanocomposites is also deduced from the first TGA derivative curves illustrated in Figure 9. The peak indicates the temperature (T_{max}) at a maximum rate of degradation. The entire first TGA derivative curves for PS nanocomposites are shifted towards right side that of pure PS, indicating higher thermal stability. The maximum degradation temperature of the pure PS is 413°C but that of the PS/organoclay nanocomposite is 437°C, indicating a 24°C improvement with just 5 wt % of clay loading. Therefore, an improvement in the thermal stability will lead to the better service performance of the nanocomposites at an elevated temperature. Similar results have also been observed by other researchers.[17,32]

Figure 10 presents the TGA curves for pure PS and PS/organoclay nanocomposites prepared with various refluxing temperature. Nanocomposite prepared at 110°C (PSNC (7, 110, 12)) has higher thermal decomposition temperature than that of the nanocomposite prepared at 25°C (PSNC (7, 25, 12)). When 50% weight loss is selected as a point of comparison, the thermal decomposition temperature for the PSNC (7, 110, 12) and PSNC (7, 25, 12) is estimated to be 427 and 425°C, respectively. Similar observation is also deduced from the first TGA derivative of PS composites depicted in Figure 11, where the peak indicates the temperature (T_{max}) at a maximum rate of degradation delayed at a higher temperature. T_{max} of the intercalated PS nanocomposite is found to be 433°C, whereas the exfoliated PS

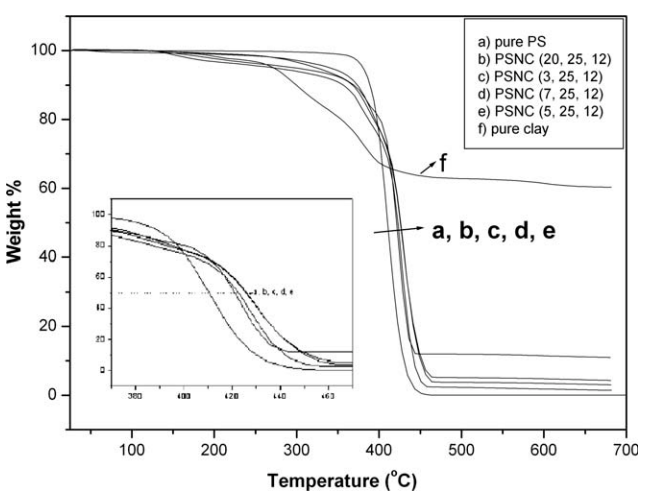

Figure 8 TGA profile for pure organoclay, pure PS and PS/organoclay nanocomposites with various contents of organoclay. Inset shows the TGA profile between 370 and 470°C.

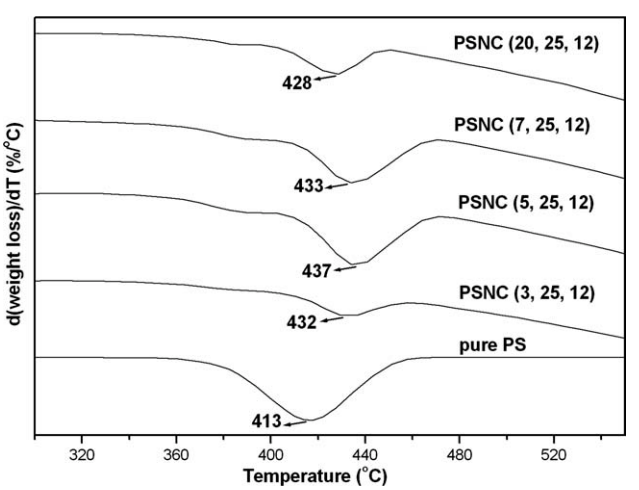

Figure 9 DTG curves for pure PS and PS/organoclay nanocomposites with different organoclay contents.

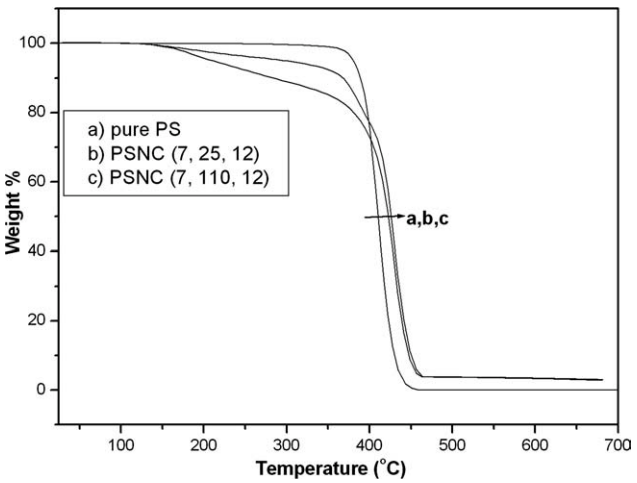

Figure 10 TGA profiles for pure PS and PS/organoclay nanocomposites prepared at different refluxing temperature.

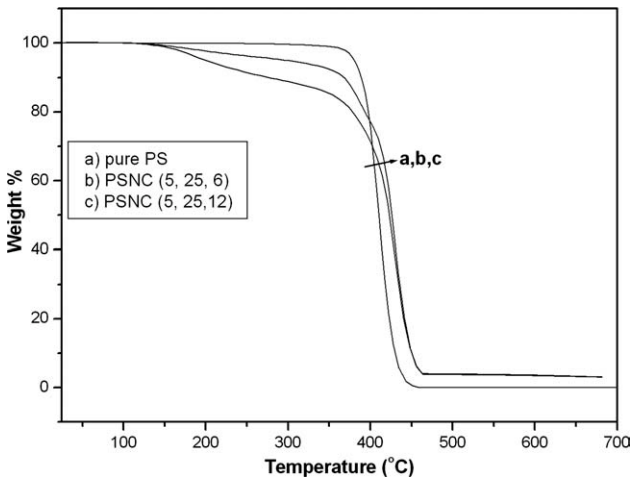

Figure 12 TGA profiles for pure PS and PS/organoclay nanocomposites prepared at different refluxing time.

nanocomposite is 440°C, indicating a 7°C improvement over the former. Figure 12 presents the TGA curves for pure PS and PS/organoclay nanocomposites prepared at different refluxing time. Nanocomposite prepared with 12-h refluxing time (PSNC (5, 25, 12)) has higher thermal decomposition temperature than that of the nanocomposite prepared with 6-h refluxing time (PSNC (5, 25, 6)). The thermal decomposition temperature for the PSNC (5, 25, 12) and PSNC (5, 25, 6) is found to be 426 and 423°C, respectively, when 50% weight loss is selected as a point of comparison. Similar observation is also deduced from the first TGA derivative of the PS nanocomposites illustrated in Figure 13. The difference of thermal behaviors can be explained by the different proportion of exfoliated and intercalated structures in these nanocomposites. The amount of exfoliated clay layers in PSNC (7, 25, 12) and PSNC (5, 25, 6) is not sufficient to promote significant improvement of the thermal stability because many of the clay layers exist as intercalated structures in this samples. Increasing the refluxing temperature from 25 to 110°C and refluxing time from 6 to 12 h lead to relatively more exfoliated clay layers, which increase the thermal stability of the nanocomposites. These results clearly indicate that the thermal stability of the exfoliated nanocomposite is better than that of intercalated composite for a constant organoclay loading. The TGA results for pure PS and PS/organoclay nanocomposites are given in Table V.

Differential scanning calorimetry

To investigate the effect of PS/organoclay ratios in the clay layers on molecular mobility of PS chains in term of its T_g (glass transition temperature), DSC study of pure PS and PS/organoclay nanocomposites has been carried out, and the results are shown

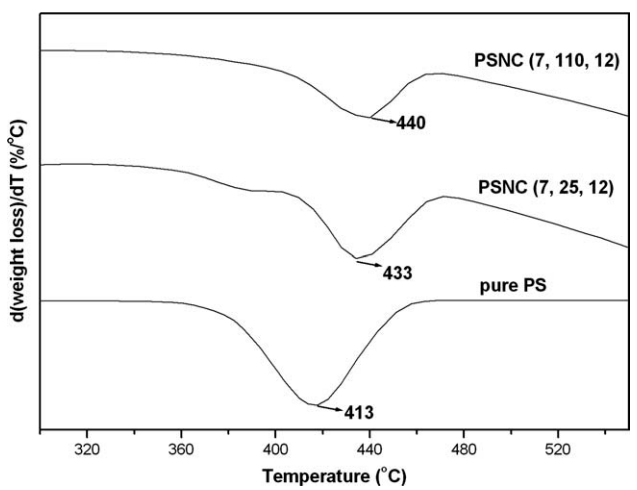

Figure 11 DTG curves for pure PS and PS/organoclay nanocomposites prepared at different refluxing temperature.

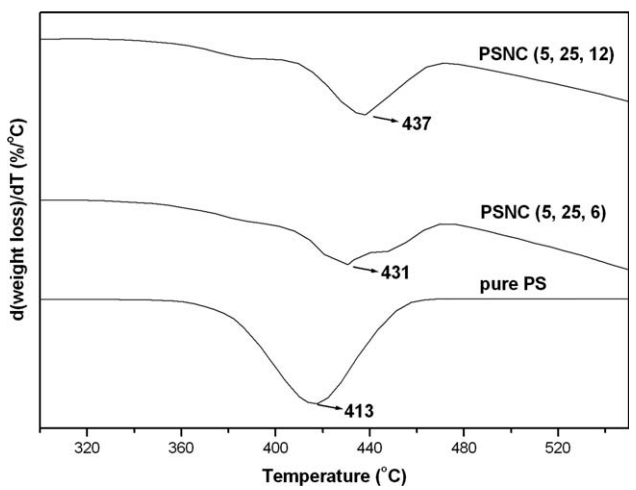

Figure 13 DTG curves for pure PS and PS/organoclay nanocomposites prepared at different refluxing time.

TABLE V
TGA Results for Pure PS and PS/Organoclay Nanocomposites

Name of sample	Temperature at 15 wt% degradation in °C°C (T_{15})	Temperature at 50 wt% degradation in °C°C (T_{50})	ΔT_{50} (°C°C)
Pure PS	393	410	------
PSNC (20, 25, 12)	386	421	11
PSNC (7, 25, 12)	384	425	15
PSNC (5, 25, 12)	382	426	16
PSNC (3, 25, 12)	373	423	13
PSNC (5, 25, 6)	375	423	13
PSNC (7, 110, 12)	386	427	17

in Figure 14. The glass transition temperature is determined at the inflection point between the onset and the end set temperatures. The T_g of the composites is remarkably increased relatively to the neat PS. The improvement in the T_g is due to the silicate nanoplatelets with high aspect ratios in the PS matrix, because the segmental motions of the polymer chains are restricted at the organic-inorganic interface, due to the confinement of the PS chains between the silicate layers and the silicate surface-polymer interaction in the nanostructured hybrids.[33] The T_g of pure PS, PS/organoclay nanocomposite samples containing 3, 5, 7, and 20 wt % of clay is determined as 68.9, 76.0, 76.1, 76.9, and 77.5°C, respectively. It is observed that the glass transition temperature of PS/organoclay nanocomposites is 7.1–8.6°C higher than that of pure PS. A very similar thermal behavior has already been reported for PS/OMMT nanocomposites, in the work done by Zidelkheir et al.[34] They reported that the improvement in T_g for PS/OMMT nanocomposites prepared by melt intercalation technique was 3°C higher than that of pure PS. According to Wang et al.,[13] the glass transition temperature of PS/OMMT nanocomposites was reported as 2.4–6.2°C higher than that of pure PS.

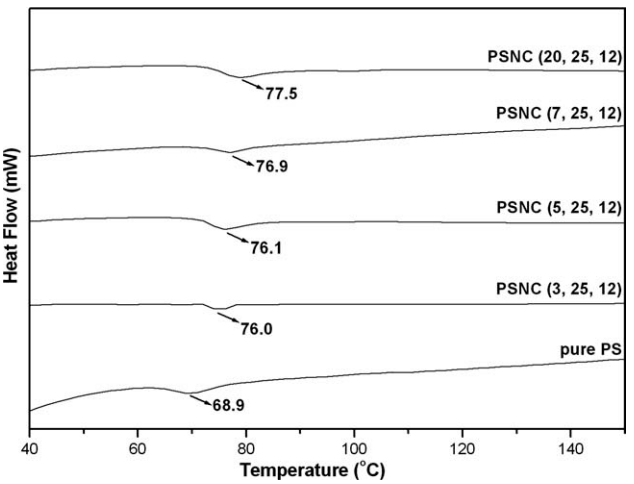

Figure 14 DSC curves for pure PS and PS/organoclay nanocomposites with various organoclay content.

Kinetic analysis using Coats-Redfern method

It is well documented[27] that Kissinger method and Flynn-Wall-Ozawa method generally used to calculate activation energy have some difficulties in calculating kinetic parameters such as reaction order, pre-exponential factor, etc. Moreover, for both methods, the range of treatment of the TG data is narrow, e.g., Kissinger model only considers one point (inflection) on the TG curve and Flynn-Wall-Ozawa model is also applicable only in a range of 5–20%. However, the Coats-Redfern method can deal with the main degradation region of TG curve of material and only requires the TG data at just one heating rate to calculate the related reaction order n, reaction activation energy E_a and pre-exponential factor A. In this work, the TG data of samples with 3, 5, 7, and 20 wt % organoclay at heating rate of 10°C/min were processed to evaluate the kinetic parameters. For this, a specified reaction order, n was assumed and then substituted the assumed n value into eq. (8). The plot of the left part of eq. (8) against $-1/T$ was fitted to calculate the correlation coefficient R. Above procedure was repeated till the best R value was obtained. The calculated reaction order at the best R value is just our required one. Subsequently, the activation energy and the pre-exponential factor can be calculated from the slope and intercept of the fitted straight line, respectively. The E_a for pure PS,

TABLE VI
Kinetic Parameters of Different Samples at the Optimum Correlation Coefficient Obtained Using Coats-Redfern Method at 10°C°C/min

Name of sample	Reaction order (n)	Activation energy (E_a kJ/mol)	Pre-exponential factor (A)	Correlation coefficient (R)
Pure PS	0.2	96	4.72×10^6	0.9996
PSNC (3, 25, 12)	0.6	185	2.25×10^{13}	0.9937
PSNC (5, 25, 12)	0.4	203	6.21×10^{14}	0.9930
PSNC (7, 25, 12)	1	186	2.59×10^{13}	0.9943
PSNC (20, 25, 12)	0.4	155	9.49×10^{10}	0.9950
PSNC (5, 25, 6)	0.4	187	2.51×10^{13}	0.9942
PSNC (7, 110, 12)	0.8	212	5.41×10^{15}	0.9943

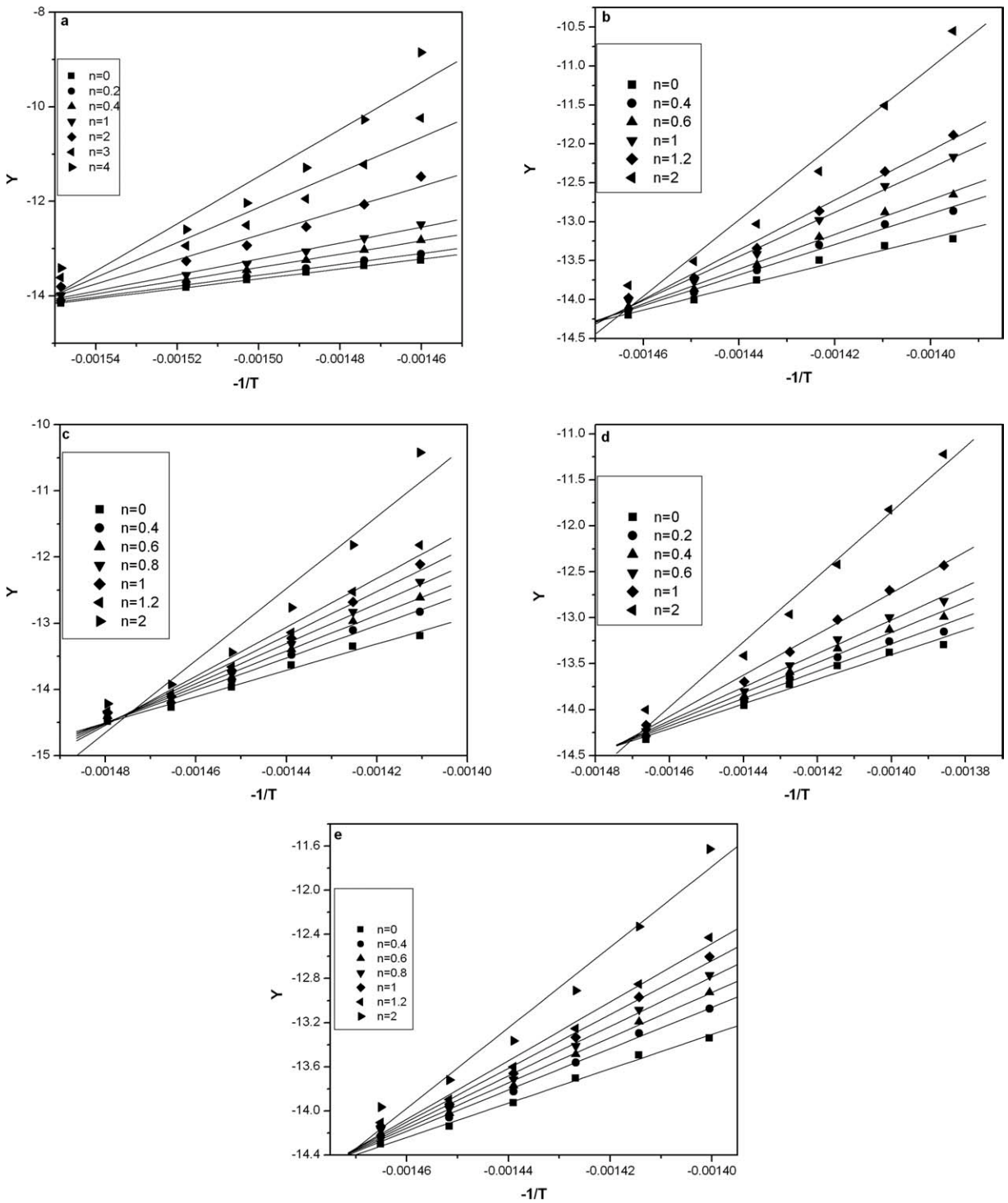

Figure 15 Determination of kinetic parameters by plots of the left part in eq. (12) against $-1/T$ using CoatseRedfern method: (a) pure PS, (b) PSNC (3, 25, 12), (c) PSNC (5, 25, 12), (d) PSNC (7, 25, 12), and e) PSNC (20, 25, 12).

PS/organoclay nanocomposites samples containing 3, 5, 7, and 20 wt % of clay is found to be 95.7, 184.9, 203.1, 185.8, and 155.6 kJ/mol, respectively. It can be seen from the Table VI that the E_a of PS/organoclay nanocomposites is 60–107 kJ/mol higher than that of pure PS, in which the PS/organoclay nanocomposite with 5 wt % has the best activation energy. Table VI also clearly indicates that the excess loading of clay (e.g., 7 and 20 wt %) can make the nanocomposites to decrease the E_a value because relatively large organic surfactant content present in the composites produces less stable charred layers during the decomposition, which is in good arrangement with the TGA data. Furthermore, the

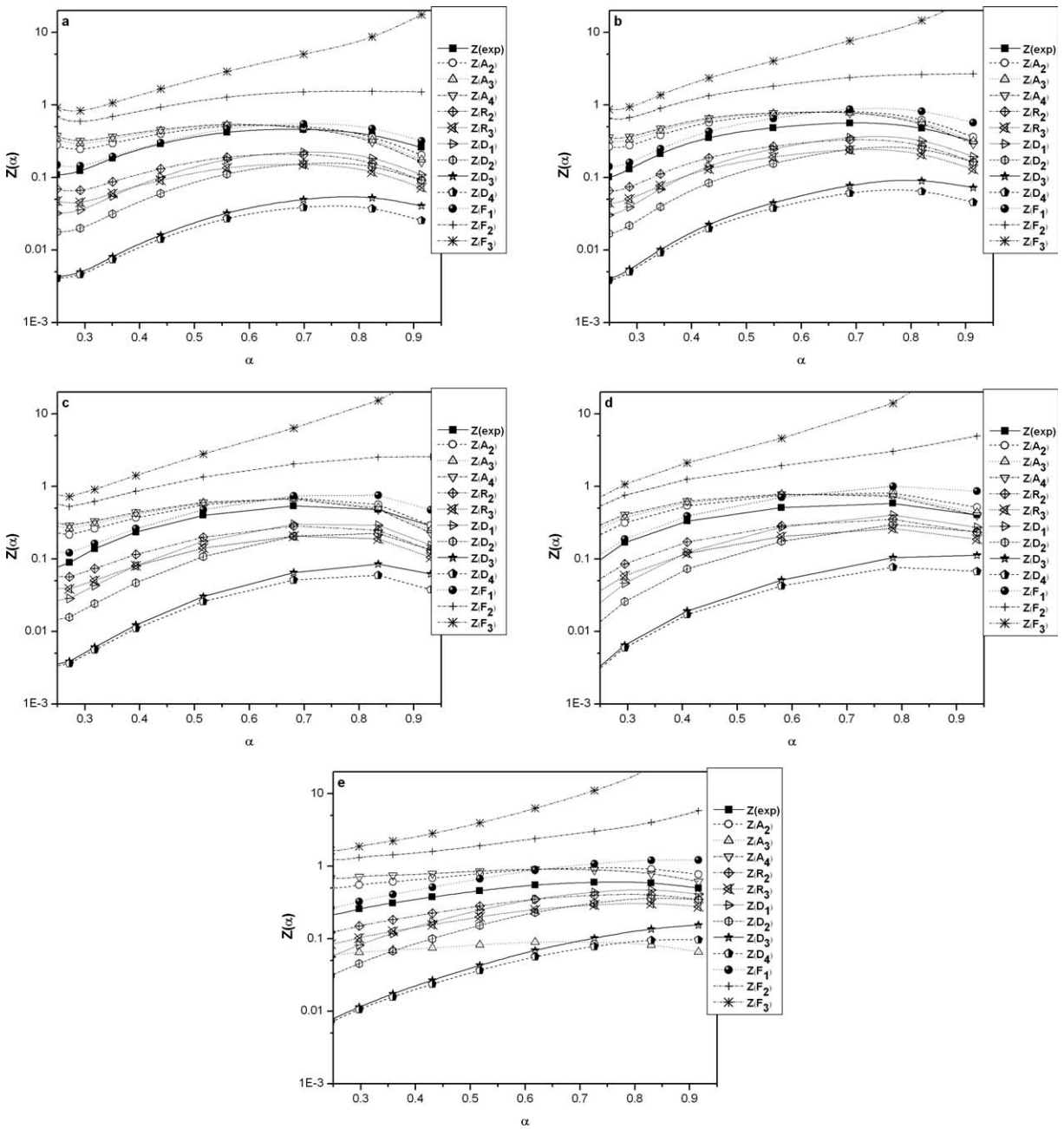

Figure 16 Determination of the thermal degradation reaction mechanism by plots of $Z(\alpha)$ versus α using Criado model: (a) pure PS, (b) PSNC (3, 25, 12), (c) PSNC (5, 25, 12), (d) PSNC (7, 25, 12), and e) PSNC (20, 25, 12).

nanocomposite samples prepared at higher temperature (110°C) and longer refluxing time (12 h) also demonstrate enhanced activation energy value, which is also consistent with TGA profile presented in Figures 10 and 12. The fitted results including reaction order, activation energy, and pre-exponential factor of the pure PS and PS nanocomposites are summarized in Table VI. Figure 15 shows the linear fitting process of pure PS and PS nanocomposite materials with different contents of organoclay at heating rate of 10°C/min, according to eq. (8). Chen et al.[27] also obtained similar kind of results for PP and the flame-retarded PP materials with IFR master batches prepared in twin-screw extruder.

Determination of the reaction mechanism of thermal degradation using Criado method

The kinetic parameters at 10°C/min heating rate obtained by Coats-Redfern method (Table VI) are substituted into Eqs. (13) and (14). The $Z(\alpha)$-α master curves can be plottedusing eq. (13), according to different reaction mechanisms $g(\alpha)$ shown in Table I. The $Z(\alpha)$-α experimental curves can also be plotted

TABLE VII
IPDTs of PS and PS/Organoclay Nanocomposites

Name of sample	A_1	A_2	A_3	T_i	T_f	IPDT
Pure PS	36,001	392	28,883	26	679	231
PSNC (3, 25, 12)	38,275	945	26,392	26	682	266
PSNC (5, 25, 12)	41,104	7179	17,104	27	680	445
PSNC (7, 25, 12)	39,968	2813	22,728	26	681	325
PSNC (20, 25, 12)	39,189	1982	24,308	27	681	299
PSNC (5, 25, 6)	34,012	7201	27,301	26	680	270
PSNC (7, 110, 12)	42,501	2810	23,425	25	681	480

using eq. (14). Figure 16(a–e) shows the $Z(\alpha)$-α master and experimental curves of pure PS and PS nanocomposite samples with 3, 5, 7, and 20 wt % organoclay. As can be seen, the experimental curve of pure PS [Fig. 16(a)] nearly overlaps the master curve of $Z(F_1)$, indicating that the thermal degradation of pure PS belongs to F_1 reaction mechanism (random nucleation having one nucleus on individual particle, i.e., the identical probability of nucleation occurring at each active site) with rate-controlling step of the nucleation process (Table I). After adding organoclay, for all PS nanocomposite samples, at the initial stage, the involved system has F_1 reaction mechanism. However, with the evolution of the thermal degradation reaction, the involved system gradually transits toward A_4 mechanism (nucleation and growth). The possible cause could be the shift of mechanism of thermal degradation at higher temperatures. Chen et al.[27] also obtained similar kind of results for PP and the flame-retarded PP materials with IFR master batches prepared in twin screw extruder.

Integral procedure decomposition temperature

The IPDT value of all PS nanocomposite samples is calculated at a constant heating rate of10°C/min, as presented in Table VII. All the nanocomposites have higher value of IPDT than the pure PS, which is an indication of higher thermal stability. The IPDT value of neat PS is 231, while that of PS nanocomposites with 3, 5, 7, and 20 wt % organoclay is 266, 445, 325, and 298, respectively. Among all, the nanocomposite prepared with 5 wt % organoclay is more stable because of highest IPDT value, which is also confirmed earlier by TGA profile (Fig. 8). The obtained IPDT results are consistent with their activation energy.

Water uptake test

The prepared PS/organoclay nanocomposite films are tested for water uptake capacity, and the results are reported in Table VIII. The water uptake capacity of the nanocomposites decreases with increasing clay content. The water uptake of pure PS film is found to be 2.20 wt %, whereas the water uptake of PS/organoclay nanocomposites with 3, 5, 7, and 20 wt % of clay is found to be 1.09, 0.98, 0.89, and 0.78 wt %, respectively. The hydrophilicity of organoclay is drastically reduced because of the effect of two influences: its treatment with the inorganic ions between the galleries by organic ions (surfactants) has displaced the outer and inner hydration shells that are coordinated to the inorganic cations, and the presence of PS chains in the interlayer space.[35,36] From these data, we can conclude that the water uptake is negligible in case of PS/organoclay nanocomposites. Hence, these nanocomposites are very much useful in preparing water proof ink and paint industry.

CONCLUSIONS

Intercalated/exfoliated PS/organoclay nanocomposites with different contents of organoclay have been synthesized via solvent blending method using xylene as a solvent. The XRD and TEM images show that the organoclay layers are well dispersed in the PS matrix. As the loading of clay increases, the intensities of the clay bands become stronger in the FTIR spectrum of PS/organoclay nanocomposites, which confirm the insertion of PS between the layers of the organoclay. The TGA result reveals that the thermal stability of PS/organoclay nanocomposites is enhanced relatively to pure PS. When 50% weight loss is selected as a comparison point, the thermal decomposition temperature of the exfoliated PS/organoclay nanocomposite with 7 wt % organoclay prepared at 110°C is 17°C higher than that of pure PS. The DSC profiles of PS/organoclay

TABLE VIII
Water Uptake Capacity of Pure PS and PS/Organoclay Nanocomposites with Different Contents of Organoclay

Name of the sample	Water uptake (wt %)
PS (0, 25, 12)	2.20
PSNC (3, 25, 12)	1.09
PSNC (5, 25, 12)	0.98
PSNC (7, 25, 12)	0.89
PSNC (20, 25, 12)	0.78

nanocomposites show a significantly enhanced glass transition temperature compared with pure PS. The glass transition temperature of PS/organoclay nanocomposites is $\sim$ 7.1–8.6°C higher than that of pure PS.

The IPDT and activation energy value of PS nanocomposites increase with an increase in the organoclay content up to 5 wt %, confirming the increase in the thermal stability of the nanocomposites. The reaction mechanism of thermal degradation of pure PS and respective nanocomposites is successfully predicted using Criado method. For the nanocomposites, at the initial stage, the involved system has F_1 reaction mechanism (random nucleation having one nucleus on individual particle, i.e., the identical probability of nucleation occurring at each active site). However, with the evolution of the thermal degradation reaction, the involved system gradually transits toward A_4 mechanism (nucleation and growth). The water uptake capacity of PS/organoclay nanocomposites is negligible when compared with pure PS and decreases with increasing the organoclay loading. Completely exfoliated nanocomposites can be achieved by decreasing the content of organoclay, increasing the refluxing temperature, and refluxing time. We believe that the solvent blending technique used in this study could be applied to prepare other intercalated/exfoliated polymer/organoclay nanocomposites.

We are grateful to Centre for Nanotechnology of IIT, Guwahati, for helping in XRD and TEM analysis and Department of Chemistry for FTIR analysis.

References

1. Park, J. H.; Jana, S. C. Polymers 2003, 44, 2091.
2. Takashi, K.; Richard, H. H.; Xing, Z.; Briber, R. M. Polymers 2004, 45, 881.
3. Utracki, L. A.; Sepehr, M.; Boccaleri, E. Polym Adv Technol 2007, 18, 1.
4. Giannelis, E. P. Adv Mater 1996, 8, 29.
5. Gilman, J. W. Appl Clay Sci 1999, 15, 31.
6. Martin, A.; Sandler, J. K. W.; Shaffer, M. S. P.; Schwarz, M. K.; Bauhofer, W.; Schulte, K. Compos Sci Technol 2004, 64, 2309.
7. Kim, T. H.; Lim, S. T.; Lee, C. H.; Choi, H. J.; Jhon, M. S. J. Appl Polym Sci 2003, 87, 2106.
8. Park, C. I. L.; Park, O. O.; Lim, J. G.; Kim, H. J. Polymers 2001, 42, 7465.
9. Ma, J.; Xu, J.; Ren, J. H.; Yu, Z. Z.; Mai, Y. W. Polymers. 2003, 44, 4619.
10. Qu, B.; Qiu, L. J Coll Interf Sci 2006, 301, 347.
11. Ding, C.; Guo, B.; He, H.; Jia, D.; Hong, H. Europ Polym J 2005, 41, 1781.
12. Qiu, L.; Chen, W.; Qu, B. Polym Degrad Stab 2005, 87, 433.
13. Wang, H. W.; Chang, K. C.; Yeh, J. M.; Joeliou, S. J Appl Polym Sci 2004, 91, 1368.
14. Wang, D.; Zhu, J.; Yao, Q.; Wilkie, A. A. Chem Mater 2002, 14, 3837.
15. Yeh, J. M.; Liou, S. J.; Lin, C. G.; Chang, Y. P.; Yu, Y. H.; Cheng, C. F. J Appl Polym Sci 2004, 92, 1970.
16. Tseng, C. R.; Wu, J. Y.; Lee, H. Y.; Chang, F. C. J Appl Polym Sci 2002, 85, 1370
17. Doh, J. G.; Cho, I. Polym Bull 1998, 41, 511
18. Liu, W. F.; Guo, Z. X.; Yu, J. J Appl Polym Sci 2005, 97, 1538.
19. Kim, M. H.; Park, C. I.; Choi, W. M.; Lee, J. W.; Lim, J. G.; Park, O. O.; Kim, J. M. J Appl Polym Sci 2004, 92, 2144.
20. Qi, R. R.; Jin, X.; Nie, J. H.; Yu, W.; Zhou, C. X. J Appl Polym Sci 2005, 97, 201.
21. Lesnikovich, A. I.; Levchik, S. V.; Levchik, G. F. J Appl Polym Sci 1986, 31, 1943.
22. Vyazovkin, S. V.; Bogdanova, V. V.; Klimovtsova, I. A.; Lesnikovich, A. I. J Appl Polym Sci 1991, 42, 2095.
23. Wu, B.; Wang, Y. Z.; Wang, X. L.; Yang, K. K.; Jin, Y. D.; Zhao, H. Polym Degrad Stab 2002, 76, 401.
24. Zhao, H.; Wang, Y. Z.; Wang, D. Y.; Wu, B.; Chen, D. Q.; Wang, X. L. Polym Degrad Stab 2003, 80, 135.
25. Wang, D. Y.; Wang, Y. Z.; Wang, J. S.; Chen, D. Q.; Zhou, Q.; Yang, B. Polym Degrad Stab 2005, 87, 171.
26. Neininger, S. M.; Staggs, J. E. J.; Horrocks, A. R.; Hill, N. J. Polym Degrad Stab 2002, 77, 187.
27. Chen, Y.; Wang, Q. Polym Degrad Stab 2007, 92, 280.
28. Wang, W. S.; Chen, H. S.; Wu, Y. W.; Tsai, T. Y.; Chen Yang, Y. W. Polymers 2008, 49, 4826.
29. Chen, W.; Qu, B. J. Mater Chem 2004, 14, 1705
30. Paul, M. A.; Alexandre, M.; Degée, P.; Henrist, C.; Rulmont, A.; Dubois, P. Polymers 2003, 44, 443
31. Alexandre, M.; Dubois, P. Mater Sci Eng 2000, 28, 1
32. Uthirakumar, P.; Song, M. K.; Changwoon, N.; Lee, Y. S. Europ Polym J 2005, 41, 211
33. Huang, J. C.; Zhu, Z.; Yin, J.; Qian, X.; Sun, Y. Y. Polymers 2001, 42, 873.
34. Zidelkheir, B.; Boudjemaa, S.; Abdel, G. M.; Djelloui, B. Polym J 2006, 15, 645.
35. Morgan, A. B.; Harries, J. D. Polymers 2004, 45, 8695
36. Zhu, A.; Cai, A.; Yu, Z.; Zhou, W. J Coll Interf Sci 2008, 322, 51.